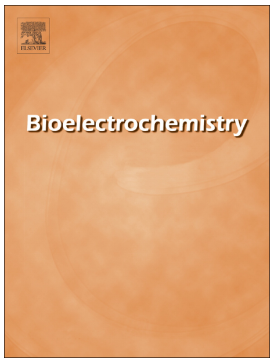

Amplified detection of leukemia cancer cells using an aptamer-conjugated gold-coated magnetic nanoparticles on a nitrogen-doped graphene modified electrode

Seyyed Mehdi Khoshfetrat, Masoud A. Mehrgardi

PII: S1567-5394(16)30233-X
DOI: doi: 10.1016/j.bioelechem.2016.12.001
Reference: BIOJEC 6982

To appear in: *Bioelectrochemistry*

Received date: 11 June 2016
Revised date: 28 November 2016
Accepted date: 8 December 2016

Please cite this article as: Seyyed Mehdi Khoshfetrat, Masoud A. Mehrgardi , Amplified detection of leukemia cancer cells using an aptamer-conjugated gold-coated magnetic nanoparticles on a nitrogen-doped graphene modified electrode. The address for the corresponding author was captured as affiliation for all authors. Please check if appropriate. Biojec(2016), doi: 10.1016/j.bioelechem.2016.12.001

Amplified Detection of Leukemia Cancer Cells Using an Aptamer-Conjugated Gold-Coated Magnetic Nanoparticles on a Nitrogen-doped Graphene Modified Electrode

Seyyed Mehdi Khoshfetrat, Masoud A. Mehrgardi*

Department of chemistry, University of Isfahan, Isfahan 81746-73441, Iran.

**Corresponding author Tel.: +98 3137934940; Fax: +98 3136689732.*

E-mail addresses: m.mehrgardi@chem.ui.ac.ir, m.mehrgardi@gmail.com.

Abstract

The increasing demands for early, accurate and ultrasensitive diagnosis of cancers demonstrate the importance of the development of new amplification strategies or diagnostic technologies. In the present study, an aptamer-based electrochemical biosensor for ultrasensitive and selective detection of leukemia cancer cells has been introduced. The thiolated sgc8c aptamer was immobilized on gold nanoparticles-coated magnetic Fe_3O_4 nanoparticles (Apt-GMNPs). Ethidium bromide (EB), intercalated into the stem of the aptamer hairpin, provides the read-out signal for the quantification of the leukemia cancer cells. After introduction of the leukemia cancer cells onto the Apt-GMNPs, the hairpin structure of the aptamer is disrupted and the intercalator molecules are released, resulting in a decrease of the electrochemical signal. The immobilization of nitrogen-doped graphene nanosheets on the electrode surface provides an excellent platform for amplifying the read-out signal. Under optimal conditions, the aptasensor exhibits a linear response over a wide dynamic range of leukemia cancer cells from 10 to 1×10^6 cell mL^{-1}. The present protocol provides a highly sensitive, selective, simple, and robust method for early stage detection of leukemia cancer. Furthermore, the fabricated aptasensor was successfully used for the detection of leukemia cancer cells in complex media such as human blood plasma, without any serious interference.

Keywords: CCRF-CEM; Cancer cell; Nitrogen-doped graphene; aptamer; Gold coated magnetic nanoparticle.

1. Introduction

Cancer is one of the most serious, lethal and frequently-occurring diseases around the world [1]. The International Agency for Research on Cancer (GLOBOCAN) has released worldwide cancer statistics, revealing 14.1 million new cancer cases, 8.2 million cancer deaths and 32.6 million people living with cancer in 2012 worldwide, and it is estimated that there will be 16 million new cases per year by 2020. Acute leukemia is a common fatal cancer that usually begins in bone marrow and results in high numbers of immature white blood cells [2]. The DNA of these cells are damaged or altered in such a way that they do not die when they should, so accumulate and occupy more and more space, ultimately, culminating in bone marrow failure [3]. Up to now, several methods have been reported for the detection of leukemia cells, such as traditional morphological analysis of the cells under an optical microscope [4], flow cytometry [5], polymerase chain reaction [6], microarray of antibodies [7], fluorescence *in situ* hybridization [8], immunohistochemistry [9] and DNA sequencing [10]. However, most of these methods are not only costly, time-consuming and labor-intensive, but also require sophisticated instrumentation and multi-step processing, and hence are not suited for routine and rapid medical analyses. Thus, the development of highly sensitive, selective, simple, and cost-effective protocols for early and accurate detection of cancer cells are of paramount importance.

The graphene nanosheet (GN), as an atomically thin and 2D graphitized structure, has opened up numerous promising opportunities in science and technology, owing to its notable properties including high effective surface area, remarkable electronic conductivity, mechanical flexibility, and ease of bio-functionalization [11, 12]. Applications of the graphene in a diverse area of science including, drug delivery [13, 14], cancer cell targeting, imaging, and therapy [15, 16] nanobiology and bioassays [17-19], energy production and storage [20] have been reported.

Doping of the GN with heteroatoms makes graphene an excellent candidate for many cutting edge applications, compared to pristine GN [21]. Incorporation of nitrogen atoms within GN (N-GN) can effectively tune its intrinsic properties including providing a much larger functional surface area, more active sites for catalytic reactions, greater electronegativy and higher electrical conductivity [22-24]. It has been reported that the high activity of N-GN may arise from the more electronegativity of nitrogen atoms in comparison with that of carbon, which results in a positive charge density on the adjacent carbon atoms [23]. Moreover, the conjugation between the nitrogen lone pair electrons and the GN π-system leads to an increase in the durability and catalytic activity of N-GN when used as supporting materials [25].

Because of good biocompatibility, high surface-to-volume ratio, and ease of surface modification, various nanostructures such as gold nanoparticles (AuNPs) [26-29], carbon nanofibers [30], titanium oxide NPs [31] and magnetic beads [32-34] have been used in electrochemical techniques to improve cancer diagnosis. Due to the superparamagnetic property of magnetic nanoparticles (MNPs) [35, 36], they can be easily retrieved from complex samples with the aid of an external magnet [37, 38]. This advantageous property reduces the possible interference and improves the figure of merit [37, 39, 40]. However, bare Fe_3O_4 NPs are not very stable and tend to aggregate easily, because of their high surface activity and large specific surface area [41-43]. These phenomena lead to poor magnetism and dispersibility, and limit their further biomedical applications [44, 45]. To overcome these drawbacks, researchers have made great efforts to coat the magnetic nanoparticles with biocompatible layers [46, 47]. Among diverse coating materials, gold has received more attention because of its unique properties such as nontoxic nature, high chemical stability and excellent biological compatibility [48-50].

Moreover, the high affinity of thiolated organic molecules to gold makes it an ideal candidate for coating of MNPs [39, 51-53].

The possibility of targeted molecular recognition plays a vital role in the development of a new generation of electrochemical biosensors. Aptamers, owing to their high affinity and selectivity towards their targets, are promising molecular recognition elements for the sensitive detection of cancer cells [1, 54]. In addition to their desirable binding capability, aptamers are important diagnostic and therapeutic molecular tools with unprecedented advantages. In contrast to traditional antibodies, aptamers are inexpensive, more stable, easy to produce and modify, and less-immunogenic or toxic [55].

Considering the low-abundance of leukemia cells at early stages, signal amplification is a central key to an earlier diagnosis and an efficient treatment [56]. One approach for signal amplification is the use of layer-by-layer (LBL) methodology [57, 58]. LBL methods can lead to accumulation of tracers on the electrode surface, thus an amplified signal [57]. Also, in the field of cancer diagnosis and therapy, LBL self-assembly has emerged as an intriguing means of cancer detection and drug delivery [59]. For example, the LBL of ferrocene-appended polyallylamine hydrochloride (Fc-PAH) functionalized graphene (Fc-PAH-G), poly(sodium-p-styrene sulfonate) (PSS), $(Fc\text{-}PAH\text{-}G/PSS)_4$, has been used for the detection of Hela cells [60]. Sun and coworkers self-assembled multi-walled carbon nanotubes (MWNTs) and AuNPs on a gold electrode using an LBL strategy for the detection of the FLT3 gene in acute myeloid leukemia (AML) [61]. Despite their generally advanced detection strategies and improved detection limits, in these methods, multilayers are interconnected through weak interactions such as hydrogen bonding, biospecific recognition, electrostatic interactions, and hydrophobic forces that limit their practical application [58]. Another important issue for sensitive cancer biosensing is the

need to decreasethe background signal to improve signal-to-background ratio (S/B) in complex media. For this purpose, in the present study, we increased S/B using gold coated MNPs (GMNPs) as both the separation tool and the immobilization support for the aptamer. Moreover, for further amplification of the signal, we modified the surface of a screen printed electrode with N-GN nanosheets. With integration of these two signal amplification strategies we introduced a simple and sensitive protocol for the detection of leukemia cells.

2. **Experimental**

2.1. Materials and apparatus

Synthetic sgc8c aptamer was purchased from Eurofins/MWG/Operon (Germany) with the following sequence: 5'-ATC TAA CTG CTG CGC CGC CGG GAA AAT ACT GTA CGG TTA GA-3'. Tris(2-carboxyethyl)phosphine (TCEP), Tetraethyl orthosilicate (TEOS), and aminopropyl triethoxy silane (APTES) were obtained from Sigma-Aldrich (USA). Sodium chloride (NaCl), potassium chloride (KCl), potassium dihydrogen phosphate (KH_2PO_4), disodium hydrogen phosphate (Na_2HPO_4), potassium ferrocyanide ($K_4Fe(CN)_6$), potassium ferricyanide ($K_3Fe(CN)_6$), sodium borohydride ($NaBH_4$), potassium permanganate ($KMnO_4$), hydrogen peroxide (H_2O_2), ethidium bromide (EB), hydrazine and nitric acid ($HNO_{3)}$ were purchased from Merck (Germany). A stock solution of the aptamer was prepared using a 1X phosphate buffer solution (PBS 1X) at pH 7 (0.01 M Na_2HPO_4, 2 mM KH_2PO4, 0.15 M NaCl and 0.15 M KCl). All the electrochemical experiments were conducted using an Autolab PGSTAT30 potentiostat/galvanostat, controlled *via* a Nova 1.8 software. Electrochemical measurements were conducted in a three-electrode cell configuration, in which a modified

carbon screen printed electrode (SPE) served as a working electrode, an Ag/AgCl/3.0 M KCl used as a reference electrode, and a Pt wire applied as a counter electrode. Electrochemical impedance spectroscopy (EIS) measurements were carried out in a solution containing $K_3Fe(CN)_6/K_4Fe(CN)_6$ (1:1, 0.5 mM) as the redox couple, with an AC voltage amplitude of 5 mV and a frequency range of 10 kHz to 0.1 Hz at an open circuit potential (OCP). Differential pulse voltammetry (DPV) was used for electrochemical detection and quantification of leukemia cancer cells over the range of 0.2 to 0.7 V at a scan rate of 20 mV s^{-1} and pulse amplitude of 25 mV. Morphological characterization and size distribution analysis of the nanoparticles was performed using a high-resolution transmission electron microscope HRTEM (Philips/CM20) operating at 300 kV. X-ray diffraction (XRD) patterns of the samples were recorded on a Bruker D8/Advance X-ray diffractometer (Germany) with Cu-Ka radiation at 40 kV and 40 mA. FT-IR spectra were recorded using a JASCO, FT/IR-6300 (Japan) spectrophotometer. Surface plasmon resonance (SPB) measurements were performed by using a JASCOV-670 UV-vis spectrophotometer. X-ray photoelectron spectroscopy (XPS) analysis was carried out using a VG Microtech Twin anode XR3E2 X-ray source (Bestec company, Germany) and a concentric hemispherical analyzer operated at a base pressure of 5×10^{-10} mbar using Al K_α ($h\upsilon$ =1486.6 eV).

2.2. Cell culture of CCRF-ECM and Ramos

CCRF-CEM (human acute lymphoblastic leukemia) and Ramos cell lines were cultured in RPMI 1640 medium supplemented with 10% fetal calf serum (FCS; Gibco 16141-079), 1% penicillin/streptomycin (Gibco 15070-063), and 2 mM L-glutamine (Gibco 25030-024). Cultures were maintained at 2×10^6 cells/ml by the addition of 50-100% fresh culture medium daily.

2.3. Synthesis of Fe_3O_4 NPs

Fe_3O_4 NPs were prepared *via* a co-precipitation step based on the procedure of Massart [62]. $FeCl_3.6H_2O$ (8.5 g) and $FeCl_2.4H_2O$ (3 g) were dissolved in deoxygenated HCl (40 mL, 0.4 M) at room temperature. NH_3 (400 mL, 0.7 M) solution was quickly added to the mixture under argon with vigorous stirring. After 30 min, magnetite precipitates were collected with a permanent magnet at the bottom of the flask, washed with deionized water, and re-dispersed in 150 mL of deionized water.

2.4. Synthesis of core–shell Fe_3O_4/SiO_2

Core–shell Fe_3O_4/SiO_2 was prepared *via* hydrolysis of TEOS in basic solution *via* Stöber's method [63] with slight modification. Briefly, 20 mL of Fe_3O_4 NPs suspension was added to 200 mL of 2-propanol and sonicated for 30 min, followed by addition of 2.24 mL ethylene glycol, 10 mL ammonia (28%), 20 mL water and 1.3 mL TEOS under vigorous stirring for 24 h. The resulting black product was sequentially washed with water and ethanol and finally dried at room temperature for 6 h.

2.5. Synthesis of aminopropyl terminated Fe_3O_4 ($Fe_3O_4/SiO_2/NH_2$)

For the synthesis of aminopropyl terminated Fe_3O_4 ($Fe_3O_4/SiO_2/NH_2$), 3 gr Fe_3O_4/SiO_2 along with 8 mL APTES were added to 30 mL of anhydrous toluene with stirring overnight under an argon atmosphere. The final product was magnetically separated, completely washed with acetone and dichloromethane, and finally dried under vacuum.

2.6. Synthesis of gold coated Fe_3O_4 NPs (GMNPs)

For preparation of the AuNP-coated magnetic NPs, 20 mg of $Fe_3O_4/SiO_2/NH_2$ was dispersed into 30 mL of water (pH 4.0) under ultrasonication for 30 min. Subsequently, 10 mL of $HAuCl_4$

aqueous solution (1.71 mM) was added to the MNPs. The gold NPs were deposited on the MNPs surface by reduction of chloroauric acid using 10 mL of $NaBH_4$ solution (0.1 M) under ultrasonication. Consequently, the nanoparticles were magnetically separated and washed using PBS 1X (pH=7.0). Details of the synthesis and TEM, XRD, FT-IR, UV-vis and EDX characterizations of different MNPs can be found in supplementary information (SI), Fig. S1.

2.7. Preparation of aptamer-conjugated GMNPs

The aptamer-conjugated GMNPs (Apt-GMNPs) were prepared *via* gold-sulfur chemistry. The S-S bond of the aptamer was deprotected by the addition of 20 μL of 0.5 mM TCEP to a 100 μL aliquot of 6 μM aptamer in the dark for 1 h. To avoid formation of the hairpin structures and undesirable hybridization between the aptamers, the solution was heated to 95 °C for 3 min, followed by cooling in an ice bath. Subsequently, 10 mg of the GMNPs was added to 100 μL of pretreated aptamer aliquot and kept for 24 h during which aptamer was self-assembled on GMNPs surface. After magnetic separation with an external magnet, the Apt-GMNP nanoconjugates were washed three times with PBS 1X (pH=7.0) to remove the unbound aptamers. Finally, the resulting Apt-GMNPs nanoconjugates were resuspended into 1.0 mL of PBS 1X (pH=7.0) buffer and stored at 4 °C.

2.8. Intercalation of EB within base pairs of aptamer

The intercalation of EB within the base pairs of immobilized aptamer occurs with the addition of 100 μL of 200 μM EB to the magnetically separated Apt-GMNPs for 3 h. The EB-aptamer was separated with the aid of an external magnet and subsequently washed with copious amount of PBS 1X (pH=7.0).

2.9. Interaction of CCRF-CEM cells with EB-aptamer

PBS solution (1.0 mL) containing different numbers of CCRF-CEM cells was added to the precipitated EB-aptamer. After 1 h incubation at 4 °C, the beads were magnetically separated to remove the supernatant and then washed three times with PBS 1X. Finally, the Apt-GMNPs-CEM was dispersed into 50 μL of PBS 1X (pH=7.0) for subsequent measurements. The control experiments were performed in a similar fashion with Ramos cells.

2.10. Preparation of Nitrogen-Doped GN

GN oxide (GO) was firstly synthesized from natural graphite powder *via* a modified Hummer's method [64] that has previously been described by our research group elsewhere [11]. Then, deoxygenated GN was prepared through a chemical reduction step [65]. To prepare N-GN [66], 5.0 mL of hydrazine monohydrate and 200 mg of deoxygenated GN were subjected to ultrasonic agitation for 1 h at 60 °C. After the sonication, a thin N-GN film was found floating at the air/water interface of the dispersion. The surface elemental composition, nitrogen bonding configurations, and the content of nitrogen were characterized using XPS (see supplementary information, Fig. S2).

2.11. Electrode preparation and electrochemical detection

Modification of the SPE was accomplished by casting 50 μL of N-GN, dispersed in water (0.5 mg mL^{-1}), on the working electrode surface (N-GN/SPE), followed by drying at room temperature. Then 50 μL of Apt-GMNPs-CEM was dropped on the N-GN/SPE. The oxidation signal of EB was monitored using DPV.

3. Results and discussion

The development of a new, simple and sensitive electrochemical detection method for leukemia cancer cells, that uses an anti-leukemia aptamer (sgc8c) as a specific recognition element, is the main goal of the present study. A general representation of the various steps of the protocol has been illustrated in Schematic 1.

Schematic 1

The Sgc8c aptamer can bind to protein tyrosine kinase 7 (PTK7), a transmembrane receptor that is over-expressed in human T-cell acute lymphocytic leukemia cells (CCRF-CEM) with a high binding affinity (K_d ~1nm) [67]. The thiolated aptamer was self-assembled on gold coated MNPs through strong Au–S linkages. Sgc8c aptamer forms a hairpin structure, consisting of a base-paired stem and an unpaired loop sequence through intramolecular base pairing [68]. EB, as a well-known intercalator, can intercalate into the double-stranded stem regions [69], thus it can be employed as an analytical probe for measuring aptamer-target interactions. After the introduction of CCRF-CEM cells, Apt-GMNPs-CEM was magnetically separated and re-suspended in a small amount of the PBS 1X (pH=7). Subsequently, the suspension was pipetted on to the N-GN modified SPE and the electrochemical oxidation signal of EB was followed by DPV. In this way, the Fe_3O_4 NPs were not only used as a separation tool for minimizing background contributions even in the presence of complex sample matrices, but also, as the strong nanocarriers for loading a high amount of aptamer that could amplify the detection signal [70]. In addition, the N-GN as a platform has demonstrated to provide excellent transduction systems for the preparation of biosensors. N-GN is a strictly two-dimensional material with highly crumpled and abundant wrinkled structures. Thus, in comparison with the smooth bare SPE, the uneven thin layer surface of the N-GN/SPE has a high specific surface area that enormously facilitates the

accessibility of more EB molecules to the electrode surface, and leads to a highly intense analytical signal [71, 72].

3.1. Electrochemical behavior of different platforms

Electrochemical impedance spectroscopy (EIS) is an effective technique to investigate the interfacial properties of the modified electrodes. Electrochemical properties of a bare SPE and those after each step of modification, including coating with GN, N-GN as well as the addition of Fe_3O_4, Fe_3O_4/SiO_2, $Fe_3O_4/SiO_2/NH_2$, and gold-coated Fe_3O_4 were studied using EIS method (Fig. 1). The charge transfer resistance (R_{ct}) of a bare SPE is relatively small, 9.8 ± 0.2 kΩ, (Fig. 1, spectrum a) and decreases to 7.7±0.2 kΩ upon the modification of SPE using GN (Fig. 1, spectrum b). Coating of SPE by N-GN dramatically decreases the R_{ct} to 71.2± 0.4 Ω), suggesting that the N-GN can considerably enhance the rate of electron transfer of the electrode (Fig. 1, spectrum c). To investigate the effect of MNPs on R_{ct}, Fe_3O_4 was pipetted on to an N-GN/SPE and the resulting R_{ct} was obtained (Fig. 1, spectrum d).When the N-GN/SPE was subjected to Fe_3O_4/SiO_2 (spectrum e) and $Fe_3O_4/SiO_2/NH_2$ (spectrum f), the values of R_{ct} were clearly increased. However, R_{ct} decreases remarkably in the case of the GMNPs/SPE (curve g).

Fig. 1

For a better understanding of the role of N-GN on the improvement of the electrochemical performance, the electrooxidation of EB was investigated on the surface of the various platforms. For this purpose, 50 µL of 200 µM of EB in 0.1 M PBS 1X (pH=7.0) was pipetted on different platforms. As shown in Fig. 2A, the anodic peak current of EB on the N-GN/SPE was increased significantly in comparison with that on a bare as well as on a GN/SPE electrode. Also, the same experiment was carried out on the different platform in the presence of 50 µL EB-aptamer in 0.1

M PBS solution (Fig. 2B). The results demonstrate that N-GN is an excellent two-dimensional substrate for improving the detection sensitivity. The presence of AuNPs, on the surface of MNPs, and their direct incorporation within the N-GN leads to the formation of an efficient electrical network that facilitates electron transfer and causes a negative shift in oxidation peak potential of the EB from 0.55 to 0.46 V (Figure 2A and B) [73]. Also, according to the previous studies [23], N-GN with pyridinic and quaternary nitrogen content enhances electron transfer efficiency. The pyridinic nitrogen in N-GN can introduce electron donor properties to GN *via* contributing two p electrons into the π system of the graphene (see the XPS analysis in the supplementary information, Fig. S2). Consequently, the metallic properties of GN resulting from the lower resistance of the N-GN is improved [21].

Fig. 2

3.2. Optimization of aptamer concentration

One of the most important steps in the fabrication of aptasensors is the determination of the amount and stability of immobilized aptamers on MNPs. Moreover, the accessibility of aptamers to the target cells plays a key role as well. Therefore, the optimal density of aptamers onto MNPs is of paramount importance to reach high sensitivity and efficiency in the response of these biosensors. On one consideration, a low density of the immobilised aptameron MNPs results in a narrow dynamic range along with a low sensitivity. Alternatively, high density of aptamer on MNPs can prevent easy accessibility to target cells due to steric hindrance, and the possibility of intermolecular hybridization [74].

To optimize the immobilization of aptamer, solutions containing different concentrations of the aptamer were immobilized on GMNPs. The oxidation signals of EB in solution containing 1×10^{3}

cell mL^{-1} CCRF-CEM (see the experimental section) were followed. As shown in Fig. 3A, with increasing the concentration of aptamer the electrochemical signals increases as well, and levels off at 10 μM of the aptamer. With further increase of the aptamer concentration, not only is the electrochemical signal not increased, it is attenuated.. As previously stated, these observations can be attributed to steric hindrances and intermolecular hybridization of the aptamers.

3.3. The effect of incubation time

The effect of incubation time of CCRF-CEM with the aptamer, immobilized on GMNPs, was also investigated and optimized. To optimize the incubation time of CCRF-CEM cells with the aptamer, a solution containing 1.0×10^{3} cells mL^{-1} was incubated with aptamer for different incubation times (Fig. 3B). The oxidation signal of EB sharply decreased with increasing incubation time and reached a plateau after 60 min.. This phenomenon can be explained in terms of the formation of a tertiary structure of aptamer-target cells at 60 min. Therefore, 60 min of incubation was chosen for the subsequent experiments.

3.4. The pH effect

The effect of pH on the electrochemical oxidation of EB was studied over the pH range from 3.0 to 9.0. For this purpose, apt-GMNP was added to 100 μL of 200 μM EB (3 h), and dissolved in PBS 1X solution of different pH values. As shown in Fig. 3C, the peak potential shifts to more negative values by increasing the pH and reaches a maximum value at pH=7.0, which is in accordance with the previously reported studies [75]. Two oxidative peaks corresponding to the two amine groups at the C3 and C8 positions of the EB molecule are observed at approximately +0.9 V and +0.5 V vs. Ag/AgCl, respectively [75]. The high oxidation potential of the amine groups in C3 overlaps with the oxidation peaks of guanine and adenine in the

aptamer sequences that can limit the specificity and selectivity of the assay. Also, high oxidation overvoltage leads to degradation of the self-assembled aptamer. Therefore, the amine group in C8 of EB, with oxidation potential of + 0.5 V, was chosen for the analyses. According to the literature [75], an oxidation of amine groups in C8 involves two electrons and one proton. Because of proton involvement in the mechanism, oxidation of amine is easier in basic media rather than in acidic ones and is associated with the shift of the anodic peak potential to more negative values. In acidic media, the double helix of DNA denatures due to protonation of the nucleotide bases. Consequently, the hairpin structures of the Sgc8c aptamer are disrupted. Also, the reduction of pH destabilizes the structure of the aptamer *via* the formation of ss-DNA with protonated cytosine (CH^+) and adenine (AH^+) bases [76]. It is obvious that the protonation of bases brings about an increase of the total positive charge, resulting in repulsion between positively charged EB and aptamer, rather than that at a neutral pH. Therefore, intercalation of EB into the aptamer decreases, and the resulting electrooxidation response reduces as well. Increase of solution pH results in destabilization of Au–S bonds and thus leads to dissociation of the aptamer from the GMNP. Moreover, comparing the binding constants of EB with dsDNA at neutral pH ($K= 1.3\times10^6\ M^{-1}$) and an acidic conditions ($K= 1.4\times10^5\ M^{-1}$) reveals a strong complexation of EB with dsDNA in physiological media [76]. Therefore, pH=7.0 was selected as the optimum condition for the detection of CCRF-CEM cells.

Fig. 3

3.5. Analytical Performance

To demonstrate that the aptasensor couuld be used for the accurate quantification of target cells, DPV peak currents of EB were recorded at various concentrations of CCRF-CEM cells under

optimal experimental conditions. The results demonstrate that as the concentration of the target cell increases, the electrochemical oxidation signal of EB progressively decreases (Fig. 4). The electrooxidation signal of EB reaches a plateau by increasing the concentration of the CCRF-CEM to 1×10^6 cells mL^{-1}. This is attributed to the occupation of all the aptamer sites on the GMNPs by the cells. The inset of Fig. 4 shows that Δi is logarithmically proportional to the concentrations of the cells over the range from 10 to 1×10^6 cells mL^{-1}, where $\Delta i=i_0-i_{cell}$; i_0 and i_{cell} represent the peak currents measured in the absence and presence of the target cells at various concentrations.

Fig. 4

Upon the introduction of CCRF-CEM cells, the aptamer will bind strongly to the cells. The formation of this complex releases EB molecules from the aptamer. In order to investigate this the hypothesis, 1×10^5 and 1×10^6 of CCRF-CEM cells in 500 μL were incubated for 1 h with the EB-aptamer solutions (as detailed in the experimental section). The beads were magnetically separated and the supernatant was carefully pipetted on the N-GN/SPE and the oxidation signal of the EB was monitored. As shown in Fig. S3, the oxidation signal of the EB from the supernatant in the absence of the cells is negligible, indicating that all the EB molecules are conjugated with aptamer and separated out from the solution with the external magnet . By increasing the cells, the oxidation responses of the EB were increased. These results clearly demonstrate that the EB molecules release from the aptamer to the solution upon the interaction of aptamer with CCRF-CEM cells.

To demonstrate that the decrease in the read-out signal only originates from the specific interaction between the aptamer and CCRF-CEM cells, not from the nonspecific interactions on

to the electrode, in a control experiment different concentrations of Ramos cells were incubated with the aptamer and the voltammograms were recorded in the same condition as that of CCRF-CEM cells. Fig. S4 demonstrates that intercalation of the EB molecules into the aptamer π-stack is stable for no significant changes in the oxidation signals of the EB molecules to be observed.

To further confirm the specific binding of the aptamer to CCRF-CEM cells, the EB-aptamer conjugate was incubated with mixed solutions of CCRF-CEM and Ramos cells with the same number concentrations (100, 1000 and 10000 cell mL^{-1}) for 1h. The resulting electrooxidation signals of EB are presented as Fig. 5. There is no significant difference in the I_{cell} and I_o currents in the presence and absence of Ramon cells. These results further confirm the specific recognition of the aptasensor for the target cells, even in a mixed medium.

Fig. 5

To investigate the capability of the aptasensor for the determination of the cancer cells in real samples, the human blood plasma samples were mixed with 1 mL of 1×10^2, 1×10^3 and 1×10^4 CCRF-CEM cells. Subsequently, the EB-Apt/GMNP was added to each solution and incubated for 1 h at 4 ^oC. After magnetic separation and washing with PBS 1X, the separated beads were dispersed in 50 μL PBS 1X (pH=7.0). The control experiments were also performed with the same concentrations of CCRF-CEM cells in a PBS 1X (pH=7) solution. The ratio of peak currents of the voltammograms for the same concentrations of the cells in PBS and serum was reported in table 1. As the results demonstrate, the signals of the cancer cells are not changed in the complex matrix.

The repeatability of the aptasensor was examined by measuring the oxidation peak currents of EB in 0.1 M PBS 1X (pH=7.0) containing 100, 1000 and 10000 cell mL^{-1}. The relative standard

deviations (RSD) of 1.8%, 2.4%, and 5.4% were obtained respectively, which implies that the reliability of the proposed method for precise quantification of the target cell (supplementary information, Fig. S5).

To demonstrate the specific intercalative interaction of EB with the immobilized aptamer, and to show the lack of any nonspecific interactions of EB with GMNPs, a 100 µL aliquot of 200 µM EB was mixed with 10 mg of GMNPs for 3 h. After the magnetic separation, GMNPs were washed with a copious amount of PBS 1X (pH=7.0). Finally, the GMNPs were dispersed into 50 µL of PBS 1X (pH=7.0) and drop cast on the N-GN/SPE. Subsequently, the electrooxidation of EB was followed using DPV with no detectable response, supporting the proposition that the specific interaction of EB with aptamer is the source of the analytical signal of the aptasensor (supplementary information, Fig. S6).

The stability of N-GN was investigated in a solution of $[Fe(CN)_6]^{3-/4-}$ (5.0 mM), containing 0.1 M KCl, by recording consecutive CVs from -0.2 to 0.6 V vs Ag/AgCl(s) at 50 mV/s. The unchanged redox peaks of N-GN after 25 cycles suggest that N-GN is strongly adsorbed onto the SPE (supplementary information, Fig. S7).

Reproducibility of the N-GN modified SPEs was investigated by recording the EIS response of four electrodes in a solution of $[Fe(CN)_6]^{3-/4-}$ (1:1, 0.5 mM) containing KCl (0.1 M). Four consecutive measurements were recorded on each electrode. The values of the R_{ct} obtained from the EIS measurements are listed in table 2. The results obtained with acceptable relative standard deviations (RSD) demonstrate the high reproducibility and excellent repeatability of the N-GN modified SPE.

4. Conclusion

An electrochemical aptasensor for selective and sensitive detection of leukemia cancer cells, based on gold-coated magnetic nanoparticles as a substrate, and nitrogen-doped graphene as the detection electrode, has been successfully fabricated. The nitrogen doped graphene shows improved electrochemical performances compared to the pristine graphene, and the bare electrode as well, that can be attributed to the higher conductivity of the N-doped graphene. The use of gold-coated magnetic nanoparticles, with a high loading of the aptamer, considerably boosts the detection sensitivity. The present aptasensor was used for the detection of leukemia cells over an extended linear dynamic range from 10 to 1×10^{6} cell mL^{-1} with a detection limit of 10 cells mL^{-1}. In addition, the sensor can differentiate between target (leukemia) and control (Ramos) cells based on the specific affinity of the aptamer to the target, leading to the applicability of the aptasensor for the detection of leukemia cells in complex media. This strategy is a promising approach and could be extended for highly sensitive and selective detection of other cancer-related cells or cancer biomarkers, with potential application in clinical analysis.

Acknowledgements

We gratefully acknowledge the support of this work by the Research Council of University of Isfahan. The authors would like to express their sincer thanks to Dr. Abolhassan Noori, for his careful editing of the manuscript. Also, the authors would like to express their deepest gratitude to Royan Institute for providing the cells.

Figure Captions

Schematic 1. Schematic illustration of the stepwise procedure for fabrication of an aptamer-based electrochemical biosensor for the detection of CCRF-CEM cells.

Fig. 1. EIS spectra of SPE in different modification steps: a) a bare SPE, b) a GN/SPE, c) an N-GN/SPE, d) Fe_3O_4/SPE, e) Fe_3O_4/SiO_2/SPE, f) Fe_3O_4/SiO_2-NH_2/SPE, g) GMNPs/SPE. Z' and Z'' are real and imaginary impedance, respectively. The spectra are recorded in 0.5 mM $[Fe(CN)_6]^{3-}$/$[Fe(CN)_6]^{4-}$ (1:1) solution.

Fig. 2. A) The electrooxidation of 200 μM EB (PBS 1X, pH=7.0) on SPE with different modification . B) The electrooxidation of EB, intercalacted into aptamer (EB-aptamer) on SPE with different modifications in a PBS 1X (pH=7.0) (a: Bare SPE; b: GN/SPE; c: N-GN/SPE).

Fig. 3. DPV responses of electrooxidation of EB in PBS 1X in different optimization steps. A) Immobilization of aptamers, B) incubation times, and C) the effect of pH (a: pH=3; b: pH=4; c: pH=5; d: pH=6; e: pH=7; f: pH=8; g: pH=9).

Fig. 4. The relationship between DPV signals and CCRF-CEM cells. The concentration of cells are 1×10^1, 1×10^2, 1×10^3, 1×10^4, 1×10^5, 1×10^6 and 6.5×10^6 cells mL^{-1}. Inset: the relationship between ΔI and the logarithms of CCRF-CEM cell numbers. The linear regression equation was $\Delta I = 0.2291 \log \text{cell} + 0.4547$, with a correlation coefficient of 0.9958.

Fig. 5. Histograms of the specificity of the assay for the detection of CCRF-CEM and Ramos cells in different concentrations.

References

[1] H.-M. Meng, H. Liu, H. Kuai, R. Peng, L. Mo, X.-B. Zhang, Aptamer-integrated DNA nanostructures for biosensing, bioimaging and cancer therapy, Chem. Soc. Rev. 45 (2016) 2583-2602.

[2] A.V. Gavai, C. Quesnelle, D. Norris, W.-C. Han, P. Gill, W. Shan, A. Balog, K. Chen, A. Tebben, R. Rampulla, D.-R. Wu, Y. Zhang, A. Mathur, R. White, A. Rose, H. Wang, Z. Yang, A. Ranasinghe, C. D'Arienzo, V. Guarino, L. Xiao, C. Su, G. Everlof, V. Arora, D.R. Shen, M.E. Cvijic, K. Menard, M.-L. Wen, J. Meredith, G. Trainor, L.J. Lombardo, R. Olson, P.S. Baran, J.T. Hunt, G.D. Vite, B.S. Fischer, R.A. Westhouse, F.Y. Lee, Discovery of Clinical Candidate BMS-906024: A Potent Pan-Notch Inhibitor for the Treatment of Leukemia and Solid Tumors, ACS Med. Chem. Lett. 6 (2015) 523-527.

[3] J. Dupuis, P. Brice, S. François, L. Ysebaert, S. de Guibert, V. Levy, S. Leprêtre, S. Choquet, M.S. Dilhuydy, L. Fornecker, V. Morel, A. Tempescul, Ofatumumab in Refractory Chronic Lymphocytic Leukemia: Experience Through the French Early Access Program, Clin. Lymphoma Myeloma Leuk. 15 (2015) e43-e46.

[4] C.S. Hourigan, J.E. Karp, Minimal residual disease in acute myeloid leukaemia, Nat. Rev. Clin. Oncol. 10 (2013) 460-471.

[5] R. Paredes-Aguilera, L. Romero-Guzman, N. Lopez-Santiago, L. Burbano-Ceron, C.D. Monte, S. Nieto-Martinez, Flow cytometric analysis of cell-surface and intracellular antigens in the diagnosis of acute leukemia, Am. J. Hematol. 68 (2001) 69-74.

[6] R. Ghossein, S. Bhattacharya, Molecular detection and characterisation of circulating tumour cells and micrometastases in solid tumours, Eur. J. Cancer 36 (2000) 1681-1694.

[7] L. Belov, O. de la Vega, C.G. dos Remedios, S.P. Mulligan, R.I. Christopherson, Immunophenotyping of leukemias using a cluster of differentiation antibody microarray, Cancer Res. 61 (2001) 4483-4489.

[8] G.W. Dewald, S.R. Brockman, S.F. Paternoster, N.D. Bone, J.R. O'Fallon, C. Allmer, C.D. James, D.F. Jelinek, R.C. Tschumper, C.A. Hanson, Chromosome anomalies detected by interphase fluorescence

in situ hybridization: correlation with significant biological features of B-cell chronic lymphocytic leukaemia, Br. J. Haematol. 121 (2003) 287-295.

[9] S.K. Singh, C. Hawkins, I.D. Clarke, J.A. Squire, J. Bayani, T. Hide, R.M. Henkelman, M.D. Cusimano, P.B. Dirks, Identification of human brain tumour initiating cells, nature 432 (2004) 396-401.

[10] T.J. Ley, E.R. Mardis, L. Ding, B. Fulton, M.D. McLellan, K. Chen, D. Dooling, B.H. Dunford-Shore, S. McGrath, M. Hickenbotham, DNA sequencing of a cytogenetically normal acute myeloid leukaemia genome, Nature 456 (2008) 66-72.

[11] S.M. Khoshfetrat, M.A. Mehrgardi, Dual amplification of single nucleotide polymorphism detection using graphene oxide and nanoporous gold electrode platform, Analyst 139 (2014) 5192-5199.

[12] S. Aznar-Cervantes, J.G. Martínez, A. Bernabeu-Esclapez, A.A. Lozano-Pérez, L. Meseguer-Olmo, T.F. Otero, J.L. Cenis, Fabrication of electrospun silk fibroin scaffolds coated with graphene oxide and reduced graphene for applications in biomedicine, Bioelectrochemistry 108 (2016) 36-45.

[13] L. Zhang, J. Xia, Q. Zhao, L. Liu, Z. Zhang, Functional graphene oxide as a nanocarrier for controlled loading and targeted delivery of mixed anticancer drugs, Small 6 (2010) 537-544.

[14] X. Wang, Q. Han, N. Yu, J. Li, L. Yang, R. Yang, C. Wang, Aptamer-conjugated graphene oxide-gold nanocomposites for targeted chemo-photothermal therapy of cancer cells, J. Mater. Chem. B 3 (2015) 4036-4042.

[15] K. Yang, L. Hu, X. Ma, S. Ye, L. Cheng, X. Shi, C. Li, Y. Li, Z. Liu, Multimodal imaging guided photothermal therapy using functionalized graphene nanosheets anchored with magnetic nanoparticles, Adv. Mater. 24 (2012) 1868-1872.

[16] O. Akhavan, E. Ghaderi, R. Rahighi, M. Abdolahad, Spongy graphene electrode in electrochemical detection of leukemia at single-cell levels, Carbon 79 (2014) 654-663.

[17] S.J. Heerema, C. Dekker, Graphene nanodevices for DNA sequencing, Nat Nano 11 (2016) 127-136.

[18] S.M. Khoshfetrat, M.A. Mehrgardi, Amplified electrochemical genotyping of single-nucleotide polymorphisms using a graphene–gold nanoparticles modified glassy carbon platform, RSC Advances 5 (2015) 29285-29293.

[19] S. Nandini, S. Nalini, M.B.M. Reddy, G.S. Suresh, J.S. Melo, P. Niranjana, J. Sanetuntikul, S. Shanmugam, Synthesis of one-dimensional gold nanostructures and the electrochemical application of the nanohybrid containing functionalized graphene oxide for cholesterol biosensing, Bioelectrochemistry 110 (2016) 79-90.

[20] F. Bonaccorso, L. Colombo, G. Yu, M. Stoller, V. Tozzini, A.C. Ferrari, R.S. Ruoff, V. Pellegrini, Graphene, related two-dimensional crystals, and hybrid systems for energy conversion and storage, Science 347 (2015) 1246501.

[21] X. Wang, G. Sun, P. Routh, D.-H. Kim, W. Huang, P. Chen, Heteroatom-doped graphene materials: syntheses, properties and applications, Chem. Soc. Rev. 43 (2014) 7067-7098.

[22] D. Deng, X. Pan, L. Yu, Y. Cui, Y. Jiang, J. Qi, W.-X. Li, Q. Fu, X. Ma, Q. Xue, Toward N-doped graphene *via* solvothermal synthesis, Chem. Mater. 23 (2011) 1188-1193.

[23] H. Wang, T. Maiyalagan, X. Wang, Review on recent progress in nitrogen-doped graphene: synthesis, characterization, and its potential applications, Acs Catalysis 2 (2012) 781-794.

[24] Q. Wen, S. Wang, J. Yan, L. Cong, Y. Chen, H. Xi, Porous nitrogen-doped carbon nanosheet on graphene as metal-free catalyst for oxygen reduction reaction in air-cathode microbial fuel cells, Bioelectrochemistry 95 (2014) 23-28.

[25] M.M. Barsan, M. David, M. Florescu, L. Ţugulea, C.M.A. Brett, A new self-assembled layer-by-layer glucose biosensor based on chitosan biopolymer entrapped enzyme with nitrogen doped graphene, Bioelectrochemistry 99 (2014) 46-52.

[26] D. Du, H. Ju, X. Zhang, J. Chen, J. Cai, H. Chen, Electrochemical immunoassay of membrane P-glycoprotein by immobilization of cells on gold nanoparticles modified on a methoxysilyl-terminated butyrylchitosan matrix, Biochemistry 44 (2005) 11539-11545.

[27] H. Li, J. Chen, S. Han, W. Niu, X. Liu, G. Xu, Electrochemiluminescence from tris (2, 2′-bipyridyl) ruthenium (II)–graphene–Nafion modified electrode, Talanta 79 (2009) 165-170.

[28] L. Ding, C. Hao, Y. Xue, H. Ju, A bio-inspired support of gold nanoparticles-chitosan nanocomposites gel for immobilization and electrochemical study of K562 leukemia cells, Biomacromolecules 8 (2007) 1341-1346.

[29] X. Wu, H. Jiang, J. Zheng, X. Wang, Z. Gu, C. Chen, Highly sensitive recognition of cancer cells by electrochemical biosensor based on the interface of gold nanoparticles/polylactide nanocomposites, J. Electroanal. Chem. 656 (2011) 174-178.

[30] C. Hao, L. Ding, X. Zhang, H. Ju, Biocompatible conductive architecture of carbon nanofiber-doped chitosan prepared with controllable electrodeposition for cytosensing, Anal. Chem. 79 (2007) 4442-4447.

[31] X. Wu, H. Jiang, Y. Zhou, J. Li, C. Wu, C. Wu, B. Chen, X. Wang, Selective determination of drug resistant cancer cells on indium tin oxide electrode modified with nano titanium dioxide, Electrochem. Commun. 12 (2010) 962-965.

[32] M. Chen, S. Bi, X. Jia, P. He, Aptamer-conjugated bio-bar-code Au–Fe 3 O 4 nanoparticles as amplification station for electrochemiluminescence detection of tumor cells, Anal. Chim. Acta. 837 (2014) 44-51.

[33] K. Zhang, T. Tan, J.-J. Fu, T. Zheng, J.-J. Zhu, A novel aptamer-based competition strategy for ultrasensitive electrochemical detection of leukemia cells, Analyst 138 (2013) 6323-6330.

[34] Y. Pan, M. Guo, Z. Nie, Y. Huang, C. Pan, K. Zeng, Y. Zhang, S. Yao, Selective collection and detection of leukemia cells on a magnet-quartz crystal microbalance system using aptamer-conjugated magnetic beads, Biosens. Bioelectron. 25 (2010) 1609-1614.

[35] E. Tombácz, R. Turcu, V. Socoliuc, L. Vékás, Magnetic iron oxide nanoparticles: Recent trends in design and synthesis of magnetoresponsive nanosystems, Biochem. Biophys. Res. Commun. 468 (2015) 442-453.

[36] H. Liu, J. Zhang, X. Chen, X.S. Du, J.L. Zhang, G. Liu, W.G. Zhang, Application of iron oxide nanoparticles in glioma imaging and therapy: From bench to bedside, Nanoscale 8 (2016) 7808-7826.

[37] D. Li, W.Y. Teoh, J.J. Gooding, C. Selomulya, R. Amal, Functionalization strategies for protease immobilization on magnetic nanoparticles, Adv. Funct. Mater. 20 (2010) 1767-1777.

[38] E. Hamidi-Asl, J.B. Raoof, M.S. Hejazi, S. Sharifi, S.M. Golabi, I. Palchetti, M. Mascini, A Genosensor for Point Mutation Detection of P53 Gene PCR Product Using Magnetic Particles, Electroanalysis 27 (2015) 1378-1386.

[39] H. Zeng, S. Sun, Syntheses, properties, and potential applications of multicomponent magnetic nanoparticles, Adv. Funct. Mater. 18 (2008) 391-400.

[40] F. Bettazzi, L. Enayati, I.C. Sánchez, R. Motaghed, M. Mascini, I. Palchetti, Electrochemical bioassay for the detection of TNF-α using magnetic beads and disposable screen-printed array of electrodes, Bioanalysis 5 (2013) 11-19.

[41] U. Jeong, X. Teng, Y. Wang, H. Yang, Y. Xia, Superparamagnetic colloids: controlled synthesis and niche applications, Adv. Mater. 19 (2007) 33-60.

[42] Q.A.M. Al-Khafaji, S. Tombelli, S. Laschi, G. Marrazza, M. Mascini, N.A.M. Mohammed, Detection of a tumor marker in serum by an electrochemical assay coupled to magnetic beads, in: Lecture Notes in Electrical Engineering, 2011, pp. 157-161.

[43] T.H. Shin, Y. Choi, S. Kim, J. Cheon, Recent advances in magnetic nanoparticle-based multi-modal imaging, Chem. Soc. Rev. 44 (2015) 4501-4516.

[44] S. Laurent, D. Forge, M. Port, A. Roch, C. Robic, L. Vander Elst, R.N. Muller, Magnetic iron oxide nanoparticles: synthesis, stabilization, vectorization, physicochemical characterizations, and biological applications, Chem. Rev. 108 (2008) 2064-2110.

[45] S.A. Majetich, T. Wen, R.A. Booth, Functional magnetic nanoparticle assemblies: Formation, collective behavior, and future directions, ACS Nano 5 (2011) 6081-6084.

[46] K. Aguilar-Arteaga, J. Rodriguez, E. Barrado, Magnetic solids in analytical chemistry: A review, Anal. Chim. Acta. 674 (2010) 157-165.

[47] I. Yildiz, Applications of magnetic nanoparticles in biomedical separation and purification, Nanotechnology Reviews 5 (2016) 331-340.

[48] S. Moraes Silva, R. Tavallaie, L. Sandiford, R.D. Tilley, J.J. Gooding, Gold coated magnetic nanoparticles: From preparation to surface modification for analytical and biomedical applications, Chem. Commun. 52 (2016) 7528-7540.

[49] I.Y. Goon, L.M.H. Lai, M. Lim, P. Munroe, J.J. Gooding, R. Amal, Fabrication and dispersion of gold-shell-protected magnetite nanoparticles: Systematic control using polyethyleneimine, Chem. Mater. 21 (2009) 673-681.

[50] S. MoraesSilva, R. Tavallaie, M. TanzirulAlam, K. Chuah, J.J. Gooding, A Comparison of Differently Synthesized Gold-coated Magnetic Nanoparticles as 'Dispersible Electrodes', Electroanalysis 28 (2016) 431-438.

[51] I. Stephanie, Core@ shell nanomaterials: gold-coated magnetic oxide nanoparticles, J. Mater. Chem. 18 (2008) 2629-2635.

[52] K.C.-F. Leung, S. Xuan, X. Zhu, D. Wang, C.-P. Chak, S.-F. Lee, W.K.-W. Ho, B.C.-T. Chung, Gold and iron oxide hybrid nanocomposite materials, Chem. Soc. Rev. 41 (2012) 1911-1928.

[53] K. Chuah, L.M.H. Lai, I.Y. Goon, S.G. Parker, R. Amal, J. Justin Gooding, Ultrasensitive electrochemical detection of prostate-specific antigen (PSA) using gold-coated magnetic nanoparticles as 'dispersible electrodes, Chem. Commun. 48 (2012) 3503-3505.

[54] J. Barman, Targeting cancer cells using aptamers: cell-SELEX approach and recent advancements, RSC Advances 5 (2015) 11724-11732.

[55] W. Zhou, P.-J. Jimmy Huang, J. Ding, J. Liu, Aptamer-based biosensors for biomedical diagnostics, Analyst 139 (2014) 2627-2640.

[56] Z. Jiang, N.D.B. Le, A. Gupta, V.M. Rotello, Cell surface-based sensing with metallic nanoparticles, Chem. Soc. Rev. 44 (2015) 4264-4274.

[57] R.R. Costa, J.F. Mano, Polyelectrolyte multilayered assemblies in biomedical technologies, Chem. Soc. Rev. 43 (2014) 3453-3479.

[58] M.M. Barsan, C.M. Brett, Recent advances in layer-by-layer strategies for biosensors incorporating metal nanoparticles, TrAC, Trends Anal. Chem. 79 (2016) 286-296.

[59] X.Q. Liu, C. Picart, Layer-by-Layer Assemblies for Cancer Treatment and Diagnosis, Adv. Mater. 28 (2016) 1295-1301.

[60] T. Wang, J. Liu, X. Gu, D. Li, J. Wang, E. Wang, Label-free electrochemical aptasensor constructed by layer-by-layer technology for sensitive and selective detection of cancer cells, Anal. Chim. Acta. 882 (2015) 32-37.

[61] Y. Sun, Q. Ren, B. Liu, Y. Qin, S. Zhao, Enzyme-free and sensitive electrochemical determination of the FLT3 gene based on a dual signal amplified strategy: Controlled nanomaterial multilayers and a target-catalyzed hairpin assembly, Biosens. Bioelectron. 78 (2016) 7-13.

[62] A. Bee, R. Massart, S. Neveu, Synthesis of very fine maghemite particles, J. Magn. Magn. Mater. 149 (1995) 6-9.

[63] W. Stöber, A. Fink, E. Bohn, Controlled growth of monodisperse silica spheres in the micron size range, J. Colloid Interface Sci. 26 (1968) 62-69.

[64] Y. Xu, H. Bai, G. Lu, C. Li, G. Shi, Flexible graphene films *via* the filtration of water-soluble noncovalent functionalized graphene sheets, J. Am. Chem. Soc. 130 (2008) 5856-5857.

[65] D. Li, M.B. Müller, S. Gilje, R.B. Kaner, G.G. Wallace, Processable aqueous dispersions of graphene nanosheets, Nat. Nanotechnol. 3 (2008) 101-105.

[66] D.-W. Wang, I.R. Gentle, G.Q.M. Lu, Enhanced electrochemical sensitivity of PtRh electrodes coated with nitrogen-doped graphene, Electrochem. Commun. 12 (2010) 1423-1427.

[67] D. Shangguan, Z. Cao, L. Meng, P. Mallikaratchy, K. Sefah, H. Wang, Y. Li, W. Tan, Cell-specific aptamer probes for membrane protein elucidation in cancer cells, J. Proteome Res. 7 (2008) 2133-2139.

[68] Y.F. Huang, D. Shangguan, H. Liu, J.A. Phillips, X. Zhang, Y. Chen, W. Tan, Molecular assembly of an aptamer–drug conjugate for targeted drug delivery to tumor cells, Chembiochem 10 (2009) 862-868.

[69] S. Minasyan, L. Tavadyan, A. Antonyan, H. Davtyan, M. Parsadanyan, P. Vardevanyan, Differential pulse voltammetric studies of ethidium bromide binding to DNA, Bioelectrochemistry 68 (2006) 48-55.

[70] F. Bettazzi, E. Hamid-Asl, C.L. Esposito, C. Quintavalle, N. Formisano, S. Laschi, S. Catuogno, M. Iaboni, G. Marrazza, M. Mascini, L. Cerchia, V. De Franciscis, G. Condorelli, I. Palchetti,

Electrochemical detection of miRNA-222 by use of a magnetic bead-based bioassay, Analytical and Bioanalytical Chemistry 405 (2013) 1025-1034.

[71] Y. Wang, Y. Li, L. Tang, J. Lu, J. Li, Application of graphene-modified electrode for selective detection of dopamine, Electrochem. Commun. 11 (2009) 889-892.

[72] J.-F. Wu, M.-Q. Xu, G.-C. Zhao, Graphene-based modified electrode for the direct electron transfer of cytochrome c and biosensing, Electrochem. Commun. 12 (2010) 175-177.

[73] A.-J. Wang, Y.-F. Li, Z.-H. Li, J.-J. Feng, Y.-L. Sun, J.-R. Chen, Amperometric glucose sensor based on enhanced catalytic reduction of oxygen using glucose oxidase adsorbed onto core-shell Fe 3 O 4@ silica@ Au magnetic nanoparticles, Mater. Sci. Eng., C 32 (2012) 1640-1647.

[74] T. Chen, M.I. Shukoor, Y. Chen, Q. Yuan, Z. Zhu, Z. Zhao, B. Gulbakan, W. Tan, Aptamer-conjugated nanomaterials for bioanalysis and biotechnology applications, Nanoscale 3 (2011) 546-556.

[75] S.C.B. Oliveira, V.B. Nascimento, Electrochemical oxidation mechanism of ethidium bromide at a glassy carbon electrode, Electroanalysis 25 (2013) 2117-2123.

[76] P.O. Vardevanyan, A.P. Antonyan, M.A. Parsadanyan, H.G. Davtyan, A.T. Karapetyan, The binding of ethidium bromide with DNA: interaction with single- and double-stranded structures, Exp Mol Med 35 (2003) 527-533.

Table 1. The ratio of peak currents of the voltammograms, for the different concentrations of the cells, in PBS and serum.

Cell Concentration (cell mL^{-1})	**Signal (in Serum)/Signal (PBS)**
0	0.98
1×10^{2}	0.97
1×10^{3}	0.95
1×10^{4}	0.96

Table 2. Reproducibility and repeatability of the different modified SPE.

Electrode	**Repeatability (% RSD)**	**Reproducibility (% RSD)**
SPE	2.04	2.04
GN/SPE	2.5	2.8
N-GN/SPE	3.6	3.7
Fe_3O_4//SPE	5.4	5.9
Fe_3O_4/SiO_2/SPE	4.6	5.02
$Fe_3O_4/SiO_2/NH_2$/SPE	5.5	6.01
GMNPs/SPE	4.8	5.1

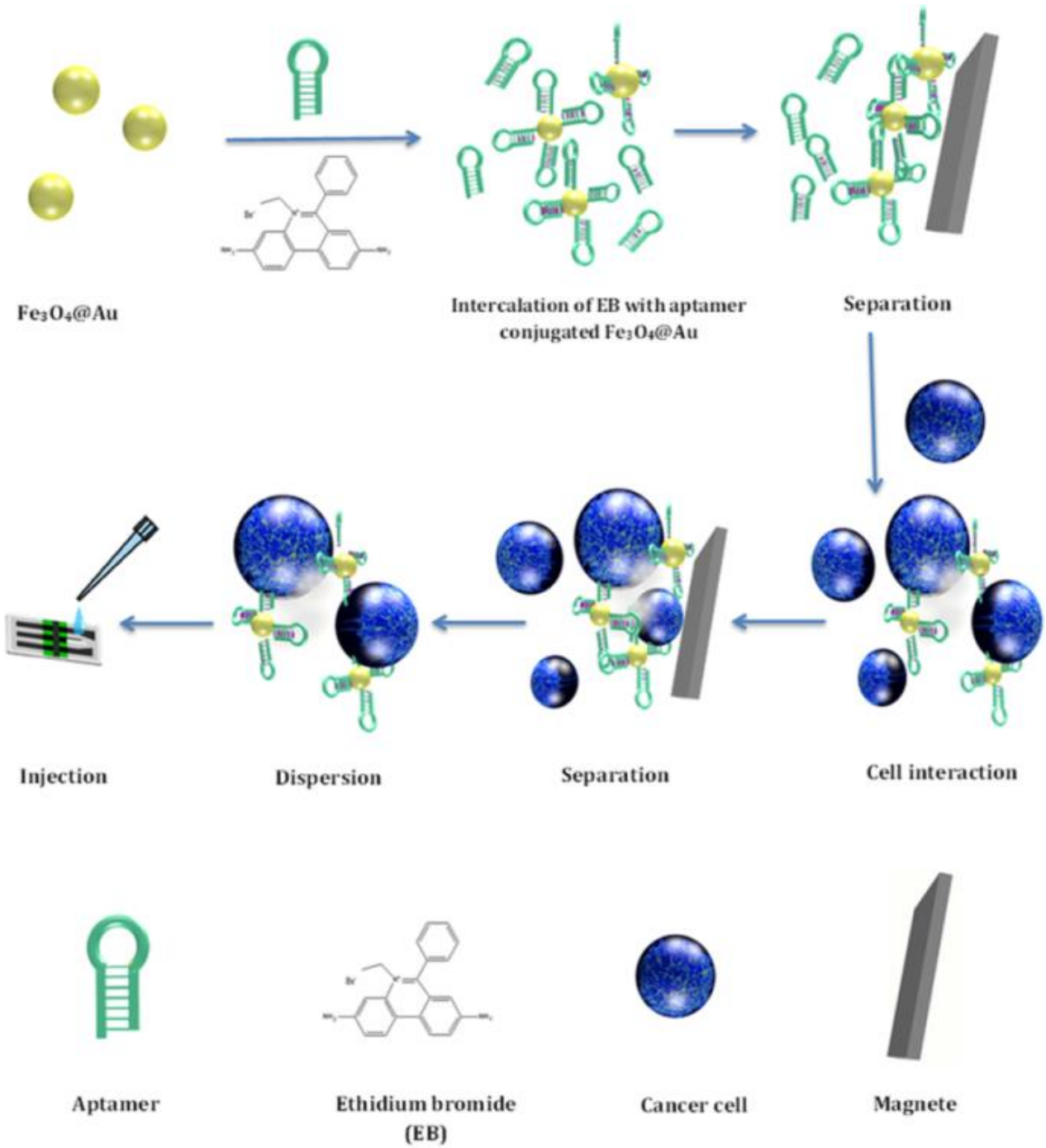

Schematic 1.

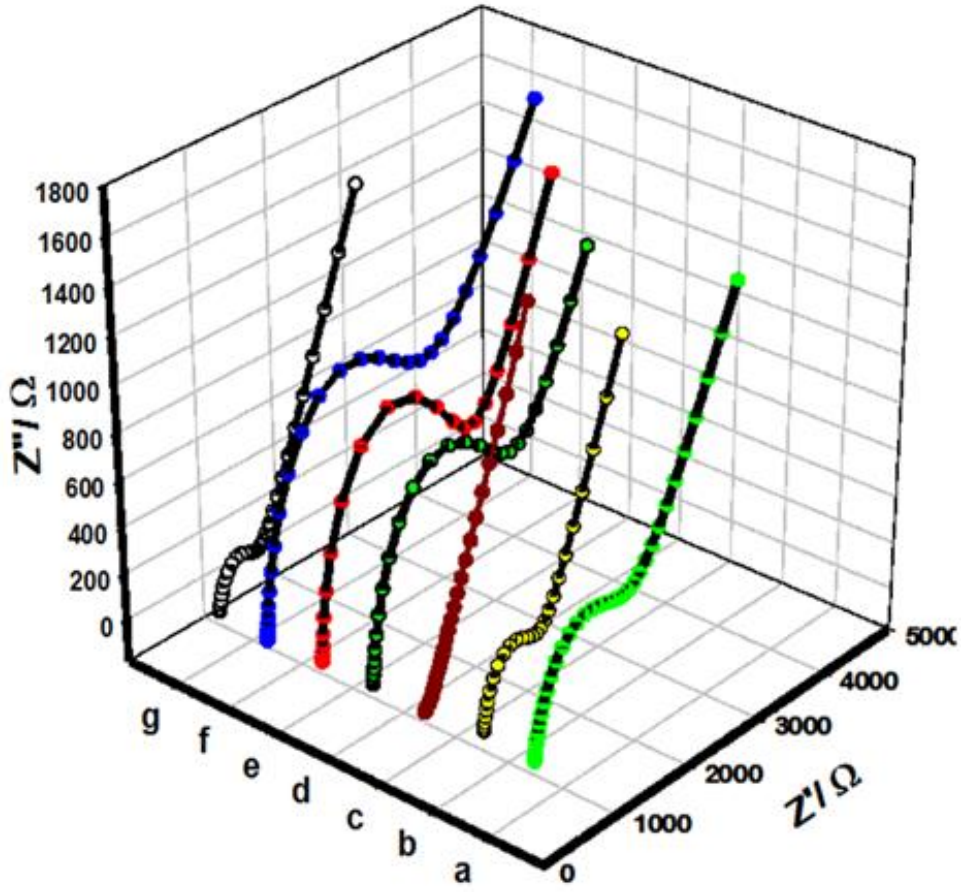

Fig. 1.

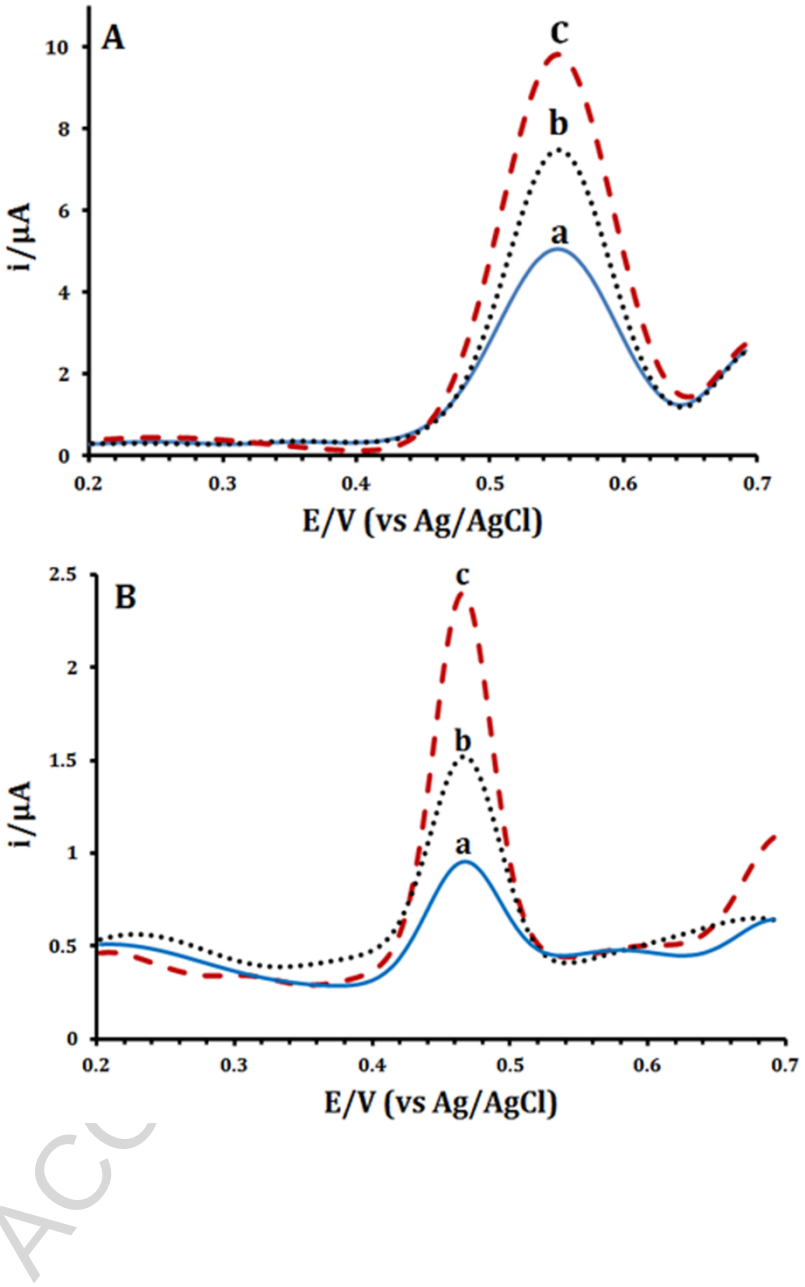

Fig. 2.

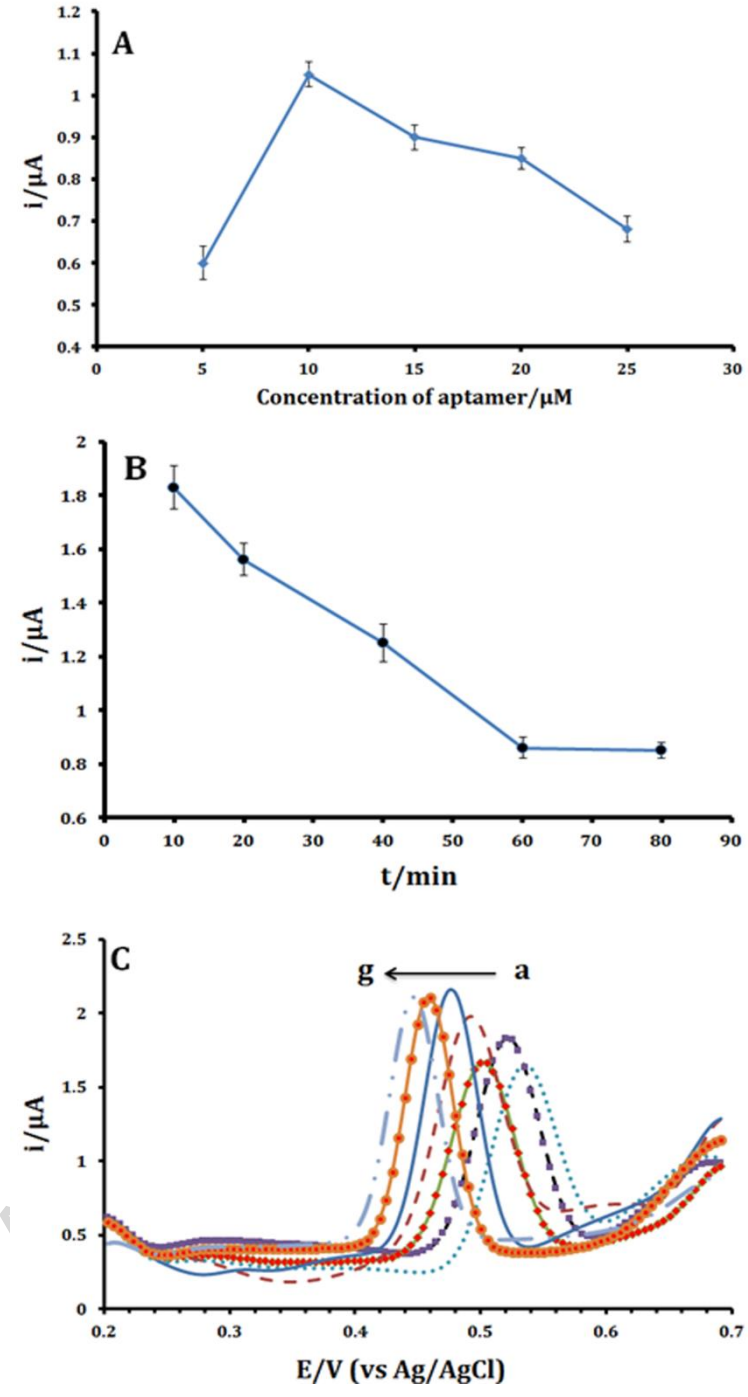

Fig. 3.

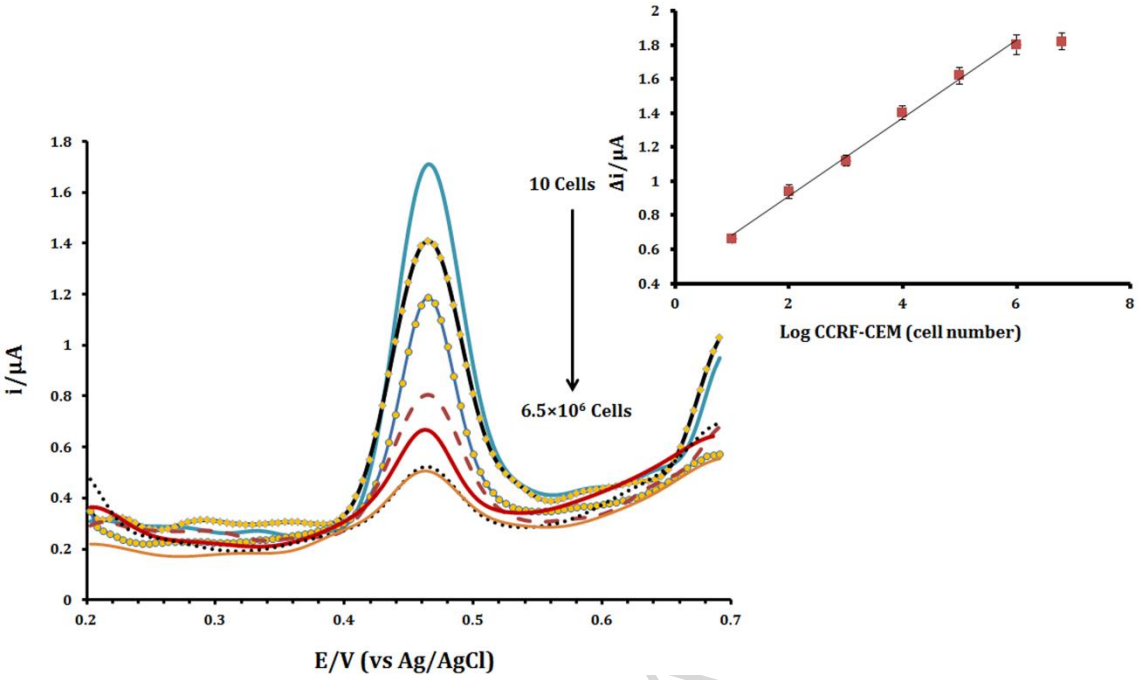

Fig. 4.

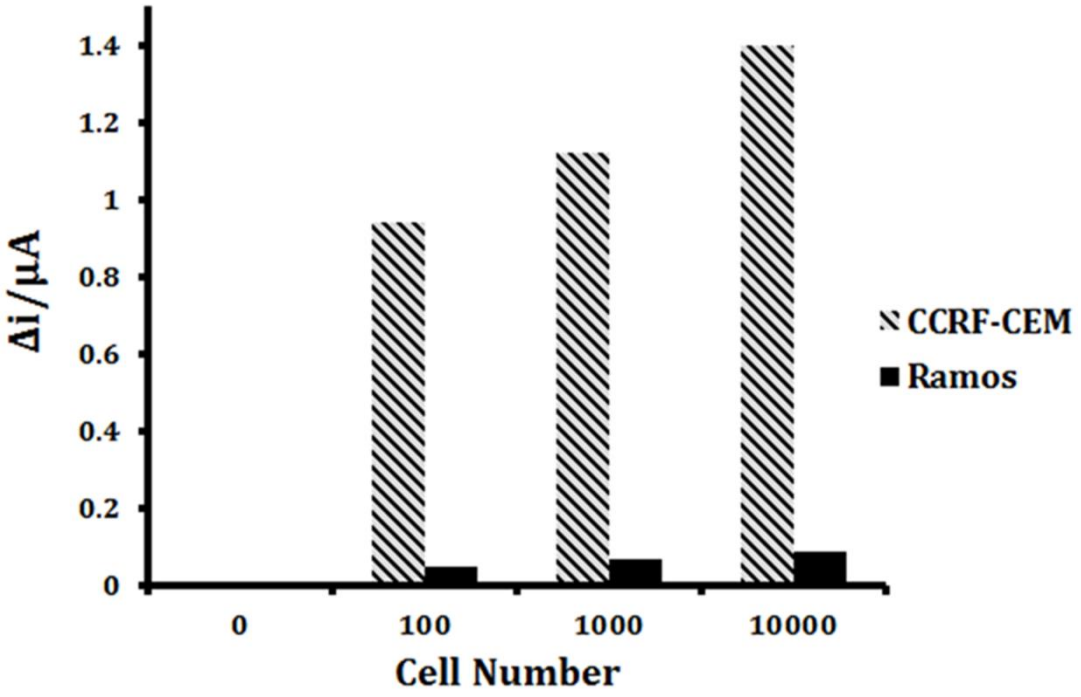

Fig. 5.

Highlights

- Nitrogen doped graphene is an excellent platform for aptasensor fabrication
- Aptamer loading was increased by applying gold coated magnetic nanoparticles
- Leukemia cell detection was achieved with a good linear dynamic range of 10–1×106 cells mL-1